Spurious Suppression Techniques for 3-D Printed Coaxial Resonator Bandpass Filters

Kunchen Zhao, *Graduate Student Member, IEEE*, and Dimitra Psychogiou, *Senior Member, IEEE*

***Abstract*— Design methods to enhance the passband-to-stopband bandwidth of coaxial bandpass filters (BPFs) are reported. Stopband enhancement is achieved by: 1) introducing a transmission zero (TZ) through mixed electromagnetic (EM) coupling and 2) by reducing the RF signal coupling to one of the spurious modes by varying the relative orientation of the RF posts. A low-cost additive manufacturing (AM) concept is proposed as the key-enabling integration scheme for these types of filters due to 1) easing the manufacturing of otherwise complex geometries and 2) allowing for monolithic integration. For proof-of-concept demonstration purposes a two-pole prototype and a four-pole prototype were designed at 3.5 and 3.6 GHz. They were manufactured using a low-cost stereolithography apparatus (SLA)-based 3-D printer. The BPFs exhibited low insertion loss (IL < 0.5 dB) and a 4.5 stopband-to-passband ratio with 35 dB rejection, which is the highest among the existing spurious-free coaxial cavity-based BPFs.**

***Index Terms*— Additive manufacturing (AM), bandpass filter (BPF), coaxial cavity filters, spurious-free filter.**

I. Introduction

THE ever crowded frequency spectrum has posed new challenges for the design of bandpass filters (BPFs) that need to exhibit not only high stopband rejection but also ultrawide stopband rejection bandwidth [1]. Spurious mode suppression techniques have been extensively studied for waveguide-based filters. In [2], the spurious band of the BPF is suppressed by cascading a lowpass filter at the cost of size and loss. In [3]–[5], the coupling to the parasitic mode is reduced by varying the orientation of the cavity resonators, leading to a stopband-to-passband ratio of $2\,f_0$ (f_0: center frequency of the fundamental mode). Other techniques using staggered harmonics resonators ($2.5\,f_0$) [6], multimode resonators ($2.6\,f_0$) [7], or introducing transmission zeros (TZs) ($1.76\,f_0$) [8] have also been proposed, however, with $<3\,f_0$ stopband ratio.

Coaxial cavity-based filters are among the most popular filtering configurations for ultrawide spurious suppression because their first spurious passband usually occurs at $3\,f_0$ [9] and they are smaller than their waveguide counterparts. BPFs comprising coaxial and dielectric resonators have been proposed to extend the stopband range of dielectric filters to $2.75\,f_0$ [10]–[12]. Techniques to enhance the stopband ratio of substrate integrated coaxial (SIC) resonator-based BPFs have also been reported [13]–[15]. In these cases, the dielectric in the coupling iris is removed to push the spurious band to higher frequencies, leading to a stopband ratio of $4.4\,f_0$. However, this method is not applicable to air-filled coaxial cavity BPFs that have significantly higher quality factor (Q) than their SIC counterparts. In [16], the harmonic of an air-filled coaxial BPF is suppressed by loading the cavity with an additional post. Nevertheless, only one spurious mode is suppressed, leading to a limited improvement of the stopband range (only $3.4\,f_0$).

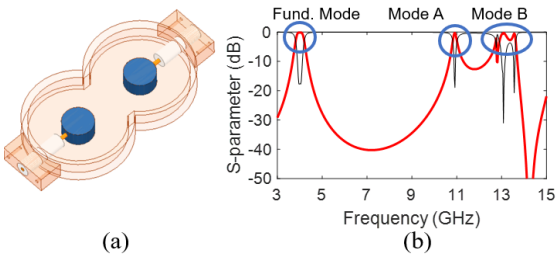

Fig. 1. Conventional two-pole coaxial cavity-resonator BPF. (a) Geometry. (b) S-parameter response plotted in a wide frequency range showing the main passband created by the fundamental mode and the two spurious bands created by Mode A and Mode B.

This letter reports on novel air-filled coaxial BPFs with ultrawide out-of-band response. Stopband enhancement is achieved by 1) introducing a TZ through mixed electromagnetic (EM) coupling and 2) by reducing the RF signal coupling to one of the spurious modes. A low-cost monolithic additive manufacturing (AM) concept is proposed to enable the fabrication of a geometrically complicated structure. A similar integration concept has been shown in [17] and [18], however, for different filter architectures that do not focus on spurious suppression techniques. The proposed spurious-suppression concept is validated through the manufacturing and testing of two- and four-pole prototypes with ultrawide passband-to-stopband ratio between 4.3 and $4.5\,f_0$.

II. Theoretical Foundations

A conventional two-pole air-filled coaxial-resonator BPF is depicted in Fig. 1 alongside its corresponding power transmission and reflection responses. It comprises the passband of interest and two spurious bands (i.e., modes A and B). The magnetic field distribution of both the main and the spurious bands are simulated using full-wave EM simulations in ANSYS HFSS and are plotted in Fig. 2. The main passband is shaped by the fundamental resonance of the capacitively-loaded coaxial resonator f_0. Mode A is generated by the resonance of the coupling iris and mode B is produced by the cylindrical cavity. To broaden the passband-to-stopband

Manuscript received August 11, 2021; accepted September 5, 2021. *(Corresponding author: Kunchen Zhao.)*

Kunchen Zhao is with the Department of Electrical, Computer and Energy Engineering, University of Colorado, Boulder, CO 80309 USA (e-mail: kunchen.zhao@colorado.edu).

Dimitra Psychogiou was with the Department of Electrical, Computer, and Energy Engineering, University of Colorado Boulder, Boulder, CO 80309 USA. She is now with the School of Engineering, University College Cork, Cork, T12 K8AF Ireland, and also with the Tyndall National Institute, Cork, T12 R5CP Ireland (e-mail: dpsychogiou@ucc.ie).

Color versions of one or more figures in this letter are available at https://doi.org/10.1109/LMWC.2021.3112406.

Digital Object Identifier 10.1109/LMWC.2021.3112406

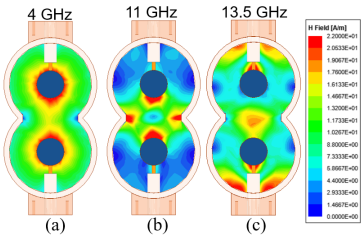

Fig. 2. Magnetic field distribution of the conventional air-filled coaxial cavity resonator BPF. (a) At $f = 4$ GHz (fundamental mode f_0) and (b) At $f = 11$ GHz (Mode A). (c) At $f = 13.5$ GHz (Mode B).

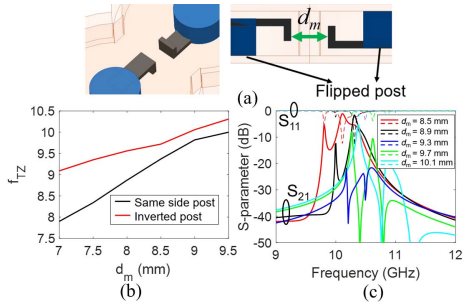

Fig. 3. (a) Geometrical details of the mixed EM coupling structures based on same-orientation posts and inverted posts. (b) Location of the TZ as a function of d_m. (c) Simulated S-parameters for Mode A when inverted posts are employed as mixed EM coupling structures showing maximum spurious suppression when $d_m = 9.3$ mm.

bandwidth of the BPF, both spurious bands need to be suppressed, which is performed as follows.

A. Suppression of Mode A

To suppress Mode A without increasing the volume of the BPF, a novel mixed EM coupling configuration is proposed to create a TZ at the location of the spurious band. It is created by inverting the coaxial posts and by adding two hooks as shown in Fig. 3(a). The magnetic coupling is provided by the iris between adjacent resonators, whereas the electrical coupling by the pair of the L-shaped conductive hooks. The strength of the electrical coupling can be adjusted by altering the size or the distance of the hooks (d_m). An inverted post configuration is used (as opposed to conventional approach based on same-orientation posts) to reduce the electrical coupling such that the TZ can be located at high frequencies, i.e., at the location of Mode A, as shown in Fig. 3(b). The TZ location can be altered by changing the electrical coupling [i.e., d_m in Fig. 3(a)]. Fig. 3(c) depicts the EM-simulated response of the filter around Mode A. As shown, the undesired spurious is canceled when the TZ is located at the frequency of Mode A (e.g., $d_m = 9.3$ mm).

B. Suppression of Mode B

As shown in Fig. 2(a) and (c), the H-filed at f_0 is evenly distributed within the volume of each resonator and is mostly higher around the post area. On the other hand, the H-field of Mode B is stronger at the location of the RF ports. Therefore, to reduce the coupling to Mode B, the RF ports can be arranged perpendicularly as shown in Fig. 4(b). Specifically, the coupling to Mode B decreased from 0.07 in the conventional in-line configuration to 0.02 in the orthogonal configuration, while the coupling to the fundamental mode remains unaffected. Therefore, the spurious band generated by Mode B can be readily suppressed by changing the port orientation.

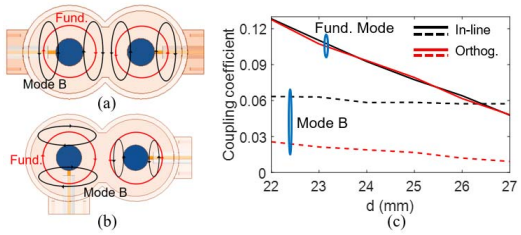

Fig. 4. Magnetic field distribution. (a) Conventional coaxial cavity BPF with in-line input–output ports. (b) Proposed BPF configuration with orthogonal port orientation for the suppression of Mode B. (c) Coupling strength for different port orientations for both the fundamental mode and Mode B.

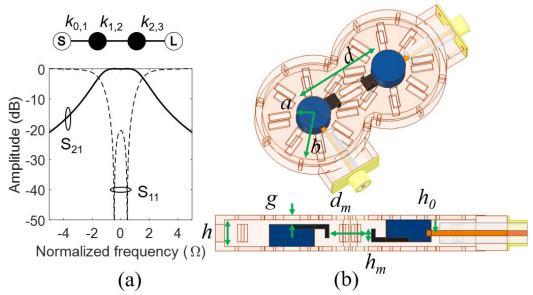

Fig. 5. (a) Coupling routing diagram and synthesized response of the proposed two-pole BPF for frequencies close to the main passband. Black circles: resonating nodes, white circles: source and load, black line: inverters. $k_{0,1} = k_{2,3} = 1$, $k_{1,2} = 1.1$. (b) Geometry of the proposed two-pole BPF. The design parameters are (in mm): $a = 5$, $b = 15$, $d = 24.5$, $g = 1$, $h = 6$, $d_m = 9.3$, $h_m = 3$, $h_0 = 3.5$.

C. Filter Design

The coupling routing diagram and its corresponding synthesized response around the main passband are shown in Fig. 5 alongside the detailed geometry of the two-pole coaxial BPF. In particular, the interresonator coupling ($k_{1,2}$) is mostly determined by the size of the coupling iris (d) and the external coupling ($k_{0,1}$) is materialized by tapping the inner conductor of the Sub-Miniature version A (SMA) to the post of the cavity, where its value is controlled by the tapping location (h_0). A small hole with depth of 1 mm is added to the post of the coaxial resonator to ensure good connection of the SMA connector. Stereolithography apparatus (SLA)-based monolithic integration approach is used for the manufacturing. To facilitate metallization of the SLA-based filter, nonradiating slots are added to the cavity wall to allow for Cu-platting. The size and location of the slots are carefully designed to minimize the radiation loss at the operating frequency as discussed in [13]. The BPF design process can be summarized as follows.

1) Design a conventional coaxial cavity filter for the main passband using the design method in [19]. Add slots for monolithic integration [13] and ensure that their size does not impact the quality factor of the filter.
2) Introduce the mixed EM-coupling in Fig. 3 and alter d_m until Mode A is suppressed as detailed in Section II-A.
3) Change the port orientation to suppress Mode B as discussed in Section II-B.

To investigate scalability of the spurious suppression concept to higher-order transfer-function, a four-resonator BPF is designed by cascading two two-resonator configurations with a 90°-long (at f_0) air-filled coaxial transmission line (TL) as shown in Fig. 6(a). Nonradiating slots are also added to the coaxial TL for Cu-plating. The impedance of the TL controls

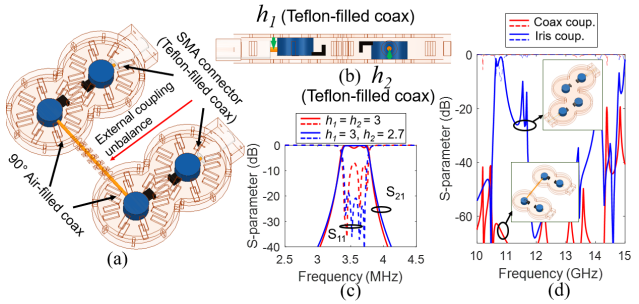

Fig. 6. (a) Geometry of the four-pole BPF using coaxial interresonator/filter coupling. (b) Side-view. (c) EM-simulated response with different coax position. (d) EM-simulated response of the four-pole BPF with iris and coaxial line-based coupling element showing spurious resonance created by the iris.

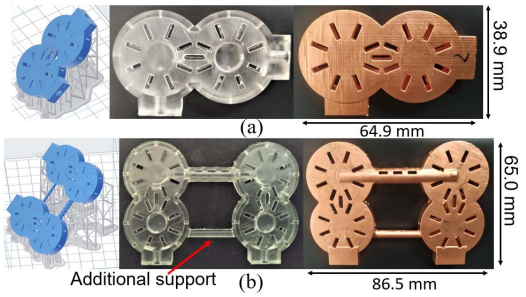

Fig. 7. Manufactured prototypes of the proposed BPF. (a) Two-pole BPF. (b) Four-pole BPF. (Left to right: 3-D printing model, before and after Cu-plating.)

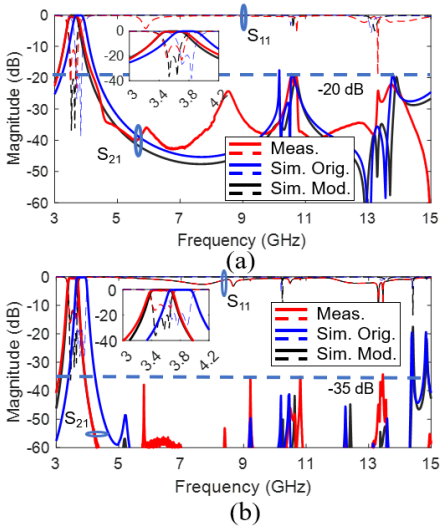

Fig. 8. RF-measured and EM-simulated S-parameters of the proposed wide-stopband filter. (a) Two-pole BPF in Fig. 7(a). (b) Four-pole BPF in Fig. 7(b).

the interfilter coupling and is chosen to be 45 Ω for optimized passband performance through parametric EM simulations. The coaxial TL cascade-type coupling-concept is preferred to the conventional iris-based one to avoid the creation of additional spurs from the iris as shown in Fig. 6(d). In this case, the external coupling of the two-resonator configuration is now shaped by a Teflon-filled SMA connector on one side and an air-filled coaxial TL on the other side. Therefore, the unbalance due to the change of the external coupling in one of the resonators needs to be compensated by altering the tapping location of the coupling elements (h_1, h_2) as shown in Fig. 6(b). The design procedure for the four-resonator BPF is as follows.

TABLE I
COMPARISON WITH THE STATE-OF-THE-ART

Ref.	#*N*	Tech.	f_c (GHz)	FBW (%)	IL (dB)	Q_{eff}	Rej. (dB)/ ratio to f_0
[5]	4	SIW	10	2.1	2.1	190	50 to 1.9 f_0
[14]	3	SIC	5	6.6	2.2	190	30 to 4.2 f_0
[15]	2	SIC	2.18-3	2.2-3	2.2	150	30 to 4.4 f_0
[16]	2	CNC	0.7	7.1	0.09	2300	30 to 3.4 f_0
[17]	2	AM	5.4	13	0.35	550	20 to 2.8 f_0
[18]	2	AM	3.5	8.8	0.08	1833	20 to 3.5 f_0
T.W.	2	AM	3.6	11.9	0.42	425	20 to 4.3 f_0
T.W.	4	AM	3.5	9.6	0.45	700	35 to 4.5 f_0

(#*N*=number of resonators, T.W.=this work, Rej.= rejection, Ref.=reference)

1) Cascade the two two-resonator BPFs using a 90° air-filled coaxial line and remove the SMA connectors between them. Optimize its impedance for optimum passband performance (45 Ω in this case) and change h_2 to compensate for the change of the external coupling as shown in Fig. 6(c).
2) Fine tune the filter dimensions with EM simulations.

III. MANUFACTURING AND TESTING

To validate the proposed spurious-suppression concept, a two-pole prototype and a four-pole prototype were designed for a center frequency of 3.8 GHz. They were manufactured using a desktop SLA 3-D printer and a commercial Cu-platting process with 50 μm copper thickness. The printing orientation and the manufactured prototypes before and after Cu-plating are shown in Fig. 7. An additional support structure is added in the four-pole filter to allow for monolithic 3-D printing and mechanical stability. The filters are characterized with a Keysight N5224A PNA, and the measured S-parameters are shown in Fig. 8 alongside their EM-simulated response. The two-pole BPF shows the following measured performance: $f_c = 3.6$ GHz, fractional bandwidth (FBW) = 11.9%, minimal insertion loss (IL) = 0.42 dB (effective quality factor $Q_{\text{eff}} = 425$), 20 dB stopband at 15.58 GHz (4.33 f_0). The four-pole BPF shows the following: $f_c = 3.5$ GHz, FBW = 9.6%, minimal IL = 0.45 dB ($Q_{\text{eff}} = 700$), 35 dB stopband at 15.63 GHz (4.47 f_0). As shown, the measured response shifted to lower frequencies due to manufacturing tolerances that required tuning by applying pressure on the upper cavity walls to compensate for variations in the capacitive gap. It was estimated to deviate by about 0.1 mm from its designed value by fitting the EM simulations to its measured S-parameters as shown in Fig. 8. A comparison with the state-of-the-art wide-stopband BPFs is listed in Table I. As shown, the proposed wide stopband technique exhibits the highest upper stopband ratio (4.47) among the reported coaxial cavity BPFs and higher Q_{eff} compared to the substrate integrated waveguide (SIW)/SIC-based filters.

IV. CONCLUSION

This letter reported on a new class of BPFs based on coaxial cavity with ultrawide passband-to-stopband bandwidth. Spurious cancellation is achieved 1) by introducing a TZ and 2) by reducing the coupling to the spurious higher order modes. The proposed BPF is validated by two prototypes manufactured using monolithic SLA printing and exhibited the highest stopband ratio among all reported coaxial cavity BPFs to date.

REFERENCES

[1] F. Teberio *et al.*, "High-power waveguide low-pass filter with all-higher-order mode suppression over a wide-band for Ka-band satellite applications," *IEEE Microw. Wireless Compon. Lett.*, vol. 25, no. 8, pp. 511–513, Aug. 2015.

[2] T.-S. Yun *et al.*, "Harmonics suppressed substrate-integrated waveguide filter with integration of low-pass filter," *Microw. Opt. Technol. Lett.*, vol. 50, no. 2, pp. 447–450, Feb. 2008.

[3] Q. Wu, F. Zhu, Y. Yang, and X. Shi, "An effective approach to suppressing the spurious mode in rectangular waveguide filters," *IEEE Microw. Wireless Compon. Lett.*, vol. 29, no. 11, pp. 703–705, Nov. 2019.

[4] J. Valencia, M. Guglielmi, S. Cogollos, and V. E. Boria, "Enhancing the out-of-band response of hybrid wide-band filters in rectangular waveguide," in *Proc. 50th Eur. Microw. Conf. (EuMC)*, Jan. 2021, pp. 747–750.

[5] P. Chu, L. Guo, L. Zhang, F. Xu, W. Hong, and K. Wu, "Wide stopband substrate integrated waveguide filter implemented by orthogonal ports' offset," *IEEE Trans. Microw. Theory Techn.*, vol. 68, no. 3, pp. 964–970, Mar. 2020.

[6] K. Zhou, C.-X. Zhou, and W. Wu, "Resonance characteristics of substrate-integrated rectangular cavity and their applications to dual-band and wide-stopband bandpass filters design," *IEEE Trans. Microw. Theory Techn.*, vol. 65, no. 5, pp. 1511–1524, May 2017.

[7] L. Qian and Q.-X. Chu, "A novel quadruple-mode cavity resonator filter with wide spurious-free window," in *IEEE MTT-S Int. Microw. Symp. Dig.*, May 2018, pp. 1–3.

[8] A. R. Azad and A. Mohan, "Substrate integrated waveguide dual-band and wide-stopband bandpass filters," *IEEE Microw. Wireless Compon. Lett.*, vol. 28, no. 8, pp. 660–662, Aug. 2018.

[9] G. L. Matthaei, "Combline band-pass filters of narrow and moderate bandwidth," *Microw. J.*, vol. 6, no. 8, pp. 82–91, Aug. 1963.

[10] A. Salehi, R. K. Reddy, T. Lukkarila, and S. Amir, "Spurious suppression of dielectric filters in practical wireless systems," in *IEEE MTT-S Int. Microw. Symp. Dig.*, Jun. 2008, pp. 1087–1090.

[11] A. R. Weily and A. S. Mohan, "Mixed combline and HE11 mode dielectric resonator filter with improved spurious performance," in *Proc. Asia–Pacific Microw. Conf.*, Hong Kong, Dec. 1997, pp. 805–808.

[12] H.-Y. Hwang, N.-S. Park, Y.-H. Cho, S.-W. Yun, and I.-S. Chang, "The design of band-pass filters made of both dielectric and coaxial resonators," in *IEEE MTT-S Int. Microw. Symp. Dig.*, Jun. 1997, pp. 805–808.

[13] B. Lee, S. Nam, B. Koh, C. Kwak, and J. Lee, "K-band frequency tunable substrate-integrated-waveguide resonator filter with enhanced stopband attenuation," *IEEE Trans. Microw. Theory Techn.*, vol. 63, no. 11, pp. 3632–3640, Nov. 2015.

[14] B. Lee, S. Nam, S.-W. Jeong, and J. Lee, "Post-loaded substrate-integrated waveguide bandpass filter with wide upper stopband and reduced electric field intensity," *IEEE Microw. Wireless Compon. Lett.*, vol. 30, no. 4, pp. 371–374, Apr. 2020.

[15] B. Lee, S. Nam, T.-H. Lee, C.-S. Ahn, and J. Lee, "Single-filter structure with tunable operating frequency in noncontiguous bands," *IEEE Trans. Compon., Packag., Manuf. Technol*, vol. 7, no. 1, pp. 98–105, Jan. 2017.

[16] E. Doumanis, "A technique to suppress harmonic outputs in coaxial cavity filters at the excitation port," *IEEE Microw. Wireless Compon. Lett.*, vol. 26, no. 11, pp. 876–878, Nov. 2016.

[17] K. Zhao and D. Psychogiou, "Monolithic SLA-based capacitively-loaded high-Q coaxial resonators and bandpass filters," in *Proc. 50th Eur. Microw. Conf. (EuMC)*, Jan. 2021, pp. 471–474.

[18] K. Zhao and D. Psychogiou, "A monolithic vertical integration concept for compact coaxial-resonator-based bandpass filters using additive manufacturing," *IEEE Microw. Wireless Compon. Lett.*, vol. 31, no. 6, pp. 689–692, Jun. 2021.

[19] G. L. Matthaei, "Comb-line band-pass filters of narrow or moderate band-width," *Microw. J.*, vol. 6, pp. 82–91, Aug. 1963.